Estimation and measurement of flat or solenoidal coil inductance for radiofrequency NMR coil design

Jan K. Rainey [1], Jeffrey S. DeVries, Brian D. Sykes *

*Protein Engineering Network of Centres of Excellence and Department of Biochemistry, University of Alberta,
419 Medical Sciences Building, Edmonton, Alta., Canada T6G 2H7*

Abstract

The inductance of a radiofrequency coil determines its compatibility with a given NMR probe circuit. However, calculation (or estimation) of inductance for radiofrequency coils of dimensions suitable for use in an NMR probe is not trivial, particularly for flat-coils. A comparison of a number of formulae for calculation of inductance is presented through the use of a straightforward inductance measurement circuit. This technique relies upon instrumentation available in many NMR laboratories rather than upon more expensive and specialized instrumentation often utilized in the literature. Inductance estimation methods are suggested and validated for both flat-coils and solenoids. These have proven very useful for fabrication of a number of new coils in our laboratory for use in static solid-state NMR probes operating at ^{1}H frequencies of 300 and 600 MHz. Solenoidal coils with very similar measured and estimated inductances having inner diameters from 1 to 5 mm are directly compared as an example of the practical application of inductance estimation for interchange of coils within an existing solid-state NMR probe.
© 2007 Elsevier Inc. All rights reserved.

Keywords: Inductance calculation; Inductance measurement; Solid-state NMR; Flat-coil; Solenoid

1. Introduction

Typically, solid-state NMR makes use of cylindrical solenoid radiofrequency coils. Such a coil is optimal for samples with a circular cross-section. In samples with inherent anisotropy, such a circular cross-section may not be optimal. For example, samples such as polymer films or solid-supported lipid bilayers will have a relatively small thickness in comparison to their length and width. The use of solenoids with a rectangular cross-section, or so-called flat-coils, for samples of this nature provides a maximal filling factor for NMR experiments [1]. Because signal intensity is directly proportional to coil filling factor [2], this optimizes signal-to-noise ratio. Following the convention

of the solid-state NMR field, we will refer to coils with a circular cross-section as solenoids and those with a rectangular cross-section as flat-coils.

It is often desirable to employ coils with different dimensions in a given static solid-state NMR probe. Prior to coil and sample fabrication, it is useful to determine ranges of dimensions which will be functional for a given probe rather than relying on trial and error. As an example, it may be desirable to test a range of conditions with small amounts of valuable sample, and then to increase the sample and coil volume once the optimal sample preparation and observation conditions are determined. In our case, we have been employing commercial two-channel static solid-state NMR probes. In each of these probes, one channel is optimized for the ^{1}H-frequency of the spectrometer and its circuitry cannot be easily modified while the second channel is configured to allow switching between different nuclei by changing capacitors within the channel circuit. Practically speaking, this means that there is a limited

---

* Corresponding author. Fax: +1 780 492 0886.
E-mail address: brian.sykes@ualberta.ca (B.D. Sykes).
[1] Present address: Department of Biochemistry and Molecular Biology, Dalhousie University, Halifax, NS, Canada B3H 1X5.

range of possible coil geometries which will function at the ^{1}H frequency for the probe. While a number of formulae are used for inductance calculation (e.g. [3,4]), these are typically optimized for coils of much larger dimensions than those employed for NMR spectroscopy, especially in the case of rectangular cross-sectional coils. This paper presents formulae for *a priori* estimation of working coil configurations for a given probe.

A typical protocol in an NMR laboratory is the testing of a new coil's resonance characteristics directly in the NMR probe using the spectrometer tuning interface. An alternate protocol allowing coil characterization without relying on the use of an NMR spectrometer is the use of a network analyzer or a sweep-generator and oscilloscope with directional coupler. This allows direct observation of the resonant frequency response of the probe circuit over a broad range of frequencies and often facilitates manipulation of the displayed data more freely. The former case ties up an NMR probe and may rely on immediate spectrometer access, which is not always desirable or possible, while the latter case uses a specialized and costly instrument not available in many NMR laboratories. Alternatively, the inductance of a given coil can be directly measured using a network analyzer with attached pickup loop (e.g. [5,6]) having known resonant properties (Dr. P.L. Gor'kov, personal communication). In order to simplify matters, we developed a highly reproducible and cost-effective method of radiofrequency coil characterization independent of having an NMR spectrometer or probe immediately available and relying only on access to an oscilloscope, sweep generator, and reflection bridge. This method uses a straightforward circuit for direct inductance measurement, which we present and use to compare coil inductance estimation methods.

2. Results and discussion

2.1. Inductance estimation

A given channel of an NMR probe acts as an oscillatory tank circuit with an inductor and capacitor in parallel (i.e. an LC-circuit) [7]. Its resonant frequency (in Hertz), v, will be given by:

$$v = \frac{1}{2\pi\sqrt{LC}} \approx \frac{1}{2\pi\sqrt{LC_{\mathrm{T}}}} \tag{1}$$

where C_{T} is the capacitance of the variable tuning capacitor (approximately equal since stray capacitance and self-capacitance of coil are being neglected) and L is the coil inductance. Therefore, the ability to calculate coil inductance provides a good estimator of its suitability for use in a given probe. A good estimator of inductance of a solenoidal coil wound on a rectangular former was derived by Niwa [4]. However, this formula, given in Appendix A, contains a summation of 12 terms based on the coil geometry, and is inconvenient to calculate. Note that the program "coil" by Moshier (available at http://www.

moshier.net/) and the Excel spreadsheet we provide (see Section 2.7) calculate this formula, allowing direct comparison with the formulae derived herein. To make inductance calculations easy to carry out for a wide variety of coil geometries and configurations, we use a fairly fundamental level of electricity and magnetism theory [8]. Details of the derivation are given in Appendix B. For a flat-coil approximated as a series of parallel current-carrying rectangles with dimensions as illustrated in Fig. 1, the estimate is:

$$L \cong \frac{4\mu_0}{\pi^2}(hw[N-1]s)$$
$$\times \left[\sum_{n=lb}^{ub} \left(\frac{w}{\sqrt{(4(ns)^2+h^2)(4(ns)^2+w^2+h^2)}} \right. \right.$$
$$\left. \left. + \frac{h}{\sqrt{(4(ns)^2+w^2)(4(ns)^2+w^2+h^2)}} \right) \right]^2 \tag{2}$$

where lb and ub are given by

$$lb = -((N-1)/2)$$
$$ub = ((N-1)/2) \tag{3}$$

for an odd number of turns N, and

$$lb = -((N-2)/2)$$
$$ub = (N/2) \tag{4}$$

for an even N. The differentiation between Eqs. (3) and (4) keeps the calculation in the centre of a turn closest to the middle of the coil, which we have found experimentally to provide a better estimate. It should be noted that a major simplification during the derivation of this formula, resulting in the overestimation of inductance, is that the magnetic field throughout the volume of the coil is taken to be that at the coil centre. In reality, there would be lower magnetic field in regions closer to the windings. This is compensated for empirically in Section 2.3.

A frequently used approximation for long inductors is
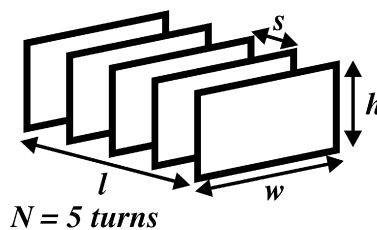
$$L \cong \frac{\mu_0 N^2 A}{l} \tag{5}$$

Fig. 1. Schematic of flat-coil with 5 turns ($N = 5$), showing definition of height (h), width (w), length (l), and turn separation ($s = l/(N - 1)$). The simplification to a series of ideal current-carrying rectangles used for inductance estimate calculation is shown.

where A is the cross-sectional area and l is the length of the inductor [3]. For a rectangular coil as defined here, this gives

$$L \cong \frac{\mu_0 N^2 h w}{[N-1]s} \tag{6}$$

The typical flat-coil used for NMR experiments has relatively few turns (4–6 is typical) and a relatively short length in comparison to its diameter, meaning that Eq. (6) is probably not a good approximation for most NMR coils. We will use both the idealized Eq. (6) and the Niwa formula (Appendix A; Eq. (A.1)) for comparison purposes.

A similar analysis to that described above for flat-coils may readily be carried out for a solenoidal coil with circular turns (Appendix B), giving the estimate

$$L \cong \frac{\mu_0 \pi r^6 [N-1]s}{4} \left[\sum_{n=lb}^{ub} \left(\frac{1}{((ns)^2 + r^2)^{3/2}} \right) \right]^2 \tag{7}$$

where r is the radius of the circular coil, and n, and s retain the same meaning as for the rectangular coil and the values lb and ub are given by Eqs. (3) and (4) for odd and even N, respectively. (Solenoids are typically reported in terms of inner diameter (id) rather than radius; we follow this convention for the remainder of the paper.) The long solenoid approximation (Eq. (5)) gives the simpler expression

$$L \cong \frac{\mu_0 \pi N^2 r^2}{[N-1]s} \tag{8}$$

which is likely less accurate for the reasons outlined above. Wheeler developed more accurate estimates for solenoids of finite length [9]—in the case of l greater than $0.8r$, this is given by:

$$L \cong \frac{10 \mu_0 \pi N^2 r^2}{9r + 10l} = \frac{10 \mu_0 \pi N^2 r^2}{9r + 10[N-1]s} \tag{9}$$

A different formula is provided by Doty [10] for l greater than $0.2r$

$$L \cong \frac{4N^2 r^2 (1 - 0.2/N)}{l + 1.2r^{0.9}} \text{ nH} \tag{10}$$

with r and l given in mm (note that Doty recommends taking r as inner radius + 20% of wire radius), which is intended to correct for the helical shape of a real solenoid. All in all, there is little consensus in the literature as to the most appropriate method to calculate a coil's inductance. The performance of each of these formulae is compared below with respect to measured inductances for a variety of solenoidal coils.

2.2. A simple inductance measurement circuit

Rather than examining changes in NMR probe response to test inductance (e.g. [11]), it is much simpler to make direct use of an LC-circuit. The circuit illustrated schematically in Fig. 2 was used, with specifications and measurement protocol as detailed in Section 4.1 and
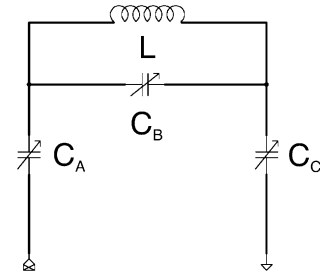

Fig. 2. Inductance measurement circuit. An inductor L (either a test coil with an unknown inductance or a commercial inductor of known inductance) is placed in parallel with variable capacitor C_B to create a simple resonant tank circuit. Variable capacitors C_A and C_C provide proper matching and balancing of the resonant circuit.

Appendix C. Using calibrated capacitors C_A, C_B and C_C, coil inductance can be determined by measurement of the circuit resonance frequency and use of Eq. (1). Note that this is more cost-effective and feasible for the average NMR laboratory than use of equipment such as a network analyzer (e.g. [12]).

Three simplifying conditions were used during circuit analysis. First, resistance of the circuit components was neglected. Second, capacitance arising from the inductor or stray capacitance in leads and wires is not taken into account. Third, self-inductance of the capacitors is not included. In order to compensate for these approximations, the circuit was calibrated using a number of known inductors. In each case, the measured inductance calculated using Eq. (1) was greater than the real inductance. This offset was dependent upon the value of C_B. Therefore, we calibrated the inductance measurements for each frequency extreme of the resonance circuit separately (Fig. 3) and report the average for each "measured inductance" value. As a whole, we estimate the uncertainty in our measurements to be 20–30 nH due primarily to factors such as variations in coil positioning or orientation relative to the remainder of the circuit and inability to exactly reproduce the soldering positions for coil legs.

2.3. Flat-coil inductance results

The suitability of the flat-coil inductance estimator (Eq. (2)) as compared to the long inductor approximation (Eq. (6)) and the Niwa formula (Appendix A; Eq. (A.1) was examined by fabrication of a number of flat-coils and measurement of their inductance using the circuit illustrated in Fig. 2 as calibrated using known inductors (Fig. 3). A variety of dimensions were chosen while the number of turns was kept in the range 4–6 (Table 1), the typical practical range of turns for flat-coil NMR. Note that six different series of coils with nearly constant dimensions but having 4, 5, and 6 turns were examined (series F1-1–F1-3 to F6-1–F6-3), three further pairs of coils with 5 and 6 turns were examined (F7-1–F7-2 to F9-1–F9-2), and two individual coils (F10 and F11) with unique dimensions. These coils cover a wide variety of coil height to width ratios. Some
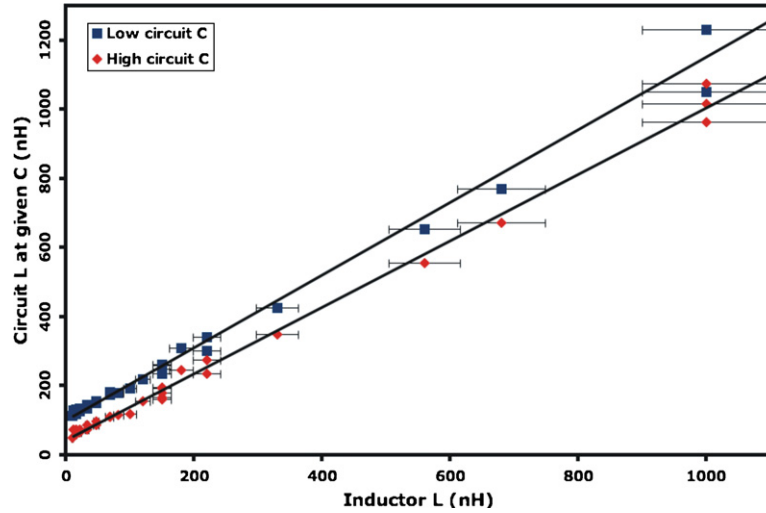
Fig. 3. Calibration of inductance measurement circuit (shown in Fig. 2) using inductors of known inductance (error bar based on tolerance of inductor). The illustrated regression lines are for the entire range of inductances. Known inductance is plotted against measured inductance. C_B in the circuit was varied between its extreme values (high and low ranges of measurements) for each inductor while C_A and C_C were left constant, providing two measured tank circuit resonant frequencies for each inductor. Effective total circuit capacitance (Eq. (13)) combined with the resonant frequency was used to determine measured inductance value (Eq. (1)). Linear regression (fit lines shown; performed on low or high effective total capacitance measurements separately) then provides a calibrated measurement of inductance for an unknown inductor examined in the same manner.

comparisons between the inductance properties for flattened vs. round copper wire and of silver vs. copper wire were also performed. Measured inductances are shown in Table 1 for each of these 29 coils and measured vs. calculated inductances are shown graphically in Fig. 4 (numerical values provided in Supplementary Material). Although major changes to wire diameter, shape and material will definitely affect coil inductance, we did not notice any systematic perturbations in inductance for the direct comparisons we performed. Our general finding to date has been that the use of different wire materials or shapes does not significantly impact inductance of the typical NMR coil; note, though, that power handling or uniformity of $\mathbf{B}_0$ within the coil may be affected by these types of changes. With small-volume coils, for example, effects of using round vs. flattened wire become more pronounced, as demonstrated by Li et al. [13].

Eq. (2) tends to overestimate flat-coil inductance, with a typical overshoot in the range of 20–30% and an extreme of ∼120 nH. As mentioned earlier, this general overestimation is most likely to be due to overestimation of the magnetic field in regions close to the windings of the coil. Eq. (6), in comparison, is seen to provide a much wider range of results, where every estimate is an overestimate. Finally, Eq. (A.1) provides reasonably good estimates in a number of cases, but tends to underestimate inductance by ∼5–30%. Examination of the performance of Eq. (2) vs. coil geometry provides an empirical manner to improve its performance. There is a definite dependence of the area and proximity of the current sheets on each pair of sides (i.e. top and bottom vs. left and right sides) of the flat-coil upon estimation accuracy. Note that this can be reduced to the ratio of coil width to height, since the length of each

side remains the same. To compensate for the different performance of Eq. (2) with variations in the width to height ratio, we propose the following as the most useful estimate of flat-coil inductance:

$$L_{\text{flat}} \approx \begin{cases} 3/7 \text{ Eq. (2)} & \text{if } 8 > w/h \geqslant 3 \text{ and } h < 2.5 \text{ mm} \\ 4/7 \text{ Eq. (2)} & \text{if } w/h \geqslant 8 \text{ and } h < 2.5 \text{ mm} \\ 11/14 \text{ Eq. (2)} & \text{if } w/h \geqslant 3 \text{ and } h \geqslant 2.5 \text{ mm} \\ \text{Eq. (2)} & \text{if } w/h < 3 \end{cases}$$

$$(11)$$

Note that we are assuming coil dimensions with $h < w$; if $h > w$, substitution of h for w and w for h in Eq. (11) should be carried out. As can be seen in Fig. 4, this estimate performs within 5% of measured inductance for 10/29 coils, within 15% for 18/29 coils, with only 5/29 coils having error of magnitude >25%. Estimates by Eq. (11) that are off by >15% range between 11 and 51 nH in magnitude of error versus measured inductance, with only four cases where this magnitude is >25 nH. (Recall that uncertainty in our measurement method is estimated at 20–30 nH.) In a recent paper, Gor'kov et al. provide a measured inductance of 80 nH for a 4-turn 8×6 mm flat-coil ∼12 mm long.[14] Eq. (11) provides an estimated inductance of 62 nH, which is a reasonably good estimate well within the uncertainty of our method. A scan of the literature provides no further reported inductance values for flat-coils, therefore further external validation of Eq. (11) is difficult. As discussed below, in practice, we find that a flat-coil having an estimated inductance using Eq. (11) on the same order as the estimated inductance of a solenoidal coil (recommended estimate given in Eq. (12)) provides a flat-coil which will work in the probe circuit.

Table 1
Flat-coil dimensions, number of turns, and measured and estimated inductances used to determine suitability of flat-coil inductance estimation formulae

Coil label	N	w (mm)	h (mm)	l (mm)	w/h	Inductance (nH)[a]
F1-1	6	15.8	5.8	12.2	2.7	273 ± 4[b]
F1-2	5	16.2	5.6	12.2	2.9	196 ± 0.9[b]
F1-3	4	15.7	6.0	12.0	2.6	143 ± 3[c]
F2-1[d]	6	19.4	4.6	17.0	4.2	237 ± 5[b]
F2-2[d]	5	20.2	5.0	16.4	4.0	169 ± 0.2[b]
F2-3[d]	4	20.2	5.1	16.4	4.0	144 ± 0.7[c]
F3-1	6	15.8	3.9	11.8	4.1	197 ± 0.1[b]
F3-2	5	15.5	3.5	12.25	4.4	141 ± 5[c]
F3-3	4	15.4	3.9	11.8	3.9	94 ± 0.8[c]
F4-1	6	15.4	1.9	11.8	8.1	134 ± 2[c]
F4-2[d]	6	15.4	1.9	12.2	8.1	111 ± 2[c]
F4-3	6	15.0	2.2	15.4	6.8	107 ± 2[c]
F4-4[e]	5	15.6	1.9	11.7	8.2	95 ± 0.9[c]
F4-5	5	15.2	2.0	12.0	7.6	88 ± 0.03[c]
F4-6	4	15.4	1.9	12.5	8.1	60 ± 5[c]
F5-1[d]	6	10.9	3.6	12.2	3.0	134 ± 1[c]
F5-2[d]	5	11.0	3.5	12.1	3.1	89 ± 0.3[c]
F5-3[d]	4	10.8	3.6	12	3.0	53 ± 2[c]
F6-1	6	9.2	1.8	17.0	5.1	42 ± 0.4[c]
F6-2	5	9.2	1.8	17.7	5.1	31 ± 2[c]
F6-3	4	9.2	1.8	15.1	5.1	18 ± 1[c]
F7-1	6	13.8	1.8	13.7	7.7	83 ± 0.1[c]
F7-2	5	13.2	1.7	16.4	7.8	54 ± 0.1[c]
F8-1	6	13.0	6.0	12.6	2.2	246 ± 2[b]
F8-2[d]	5	12.4	5.5	12.6	2.3	165 ± 3[b]
F9-1[d]	6	11.8	4.6	11.5	2.6	195 ± 0.5[b]
F9-2[d]	6	12.3	4.4	13.6	2.8	157 ± 3[b]
F10	6	20.3	3.8	16.5	5.3	200 ± 2[b]
F11[d]	4	12.8	2.8	12	4.6	55 ± 3[c]

All dimensions (see Fig. 1) are for the interior of the coil except length which is leg-to-leg distance. Unless otherwise indicated, all coils were fabricated with 20 AWG copper wire.

[a] Errors are given based upon the paired measurements made at high and low total capacitance for the measurement circuit. Uncertainty in inductance measurement is ~20–30 nH.

[b] Inductance calibrated by linear regression over 0–1.0 μH range of inductors (Fig. 3).

[c] Inductance calibrated by linear regression over 0–150 nH range of inductors (Fig. 3).

[d] Flattened 20 AWG copper wire.

[e] 19 AWG silver wire.

2.4. Solenoidal coil inductance results

A total of 24 solenoidal coils with a variety of id's, lengths, and numbers of turns were fabricated and inductances were measured using the circuit illustrated in Fig. 2, as described in Section 4.1. Coil parameters along with measured inductances are given in Table 2. Fig. 5 shows measured vs. calculated inductance for: (1) the formula derived in the same manner as for the flat-coil (Eq. (7)); (2) the long-inductor formula (Eq. (8)); (3) Wheeler's inductor of finite length (Eq. (9)); and, (4) Doty's inductance estimation formula (Eq. (10)). Generally, Eq. (9) provides an excellent estimate for coils of any id over the range measured of 1–10 mm. Eq. (7) tends to severely underestimate inductance for diameters of 5 mm and greater, but performs about equally well to Eq. (9) for the smaller diameters. Eq. (10) performs similarly to Eq. (9), but Eq. (9) tends to be more consistent with our measurements of coil inductance. Finally, Eq. (8), which is notably a frequently encountered formula for inductance calculation, does not provide a consistent inductance estimate in the regime of NMR solenoidal coils.

Based upon these results, we suggest that Eqs. (7) and (9) be directly compared at coil diameters of ≲ 5 mm, with the inductance estimate given by the following expression:

$$L_{\text{solenoid}} \approx \begin{cases} \text{Eq. (7)} & \text{if } 3/4 \text{ Eq. (7)} > \text{Eq. (9)} \\ \text{Eq. (9)} & \text{if Eq. (9)} > 4/3 \text{ Eq. (7)} \\ \frac{\text{Eq. (7)} + \text{Eq. [9]}}{2} & \text{if } 3/4 \text{ Eq. (7)} < \text{Eq. (9)} < 4/3 \text{ Eq. (7)} \end{cases}$$

(12)

Note that Eq. (12) will almost always result in Eq. (9) for larger diameters where Eq. (7) provides an underestimate. To be certain of the better estimate at diameters of 5 mm and above, however, Eq. (9) should be used without reference to Eq. (12). Following this estimation procedure, the results shown in Fig. 5 demonstrate that a good estimation of inductance was provided for all coils tested. Of the 24 coils tested, 11/24 were predicted at <5% error and 19/24 at 15% error or better, with the remaining 5 coils at
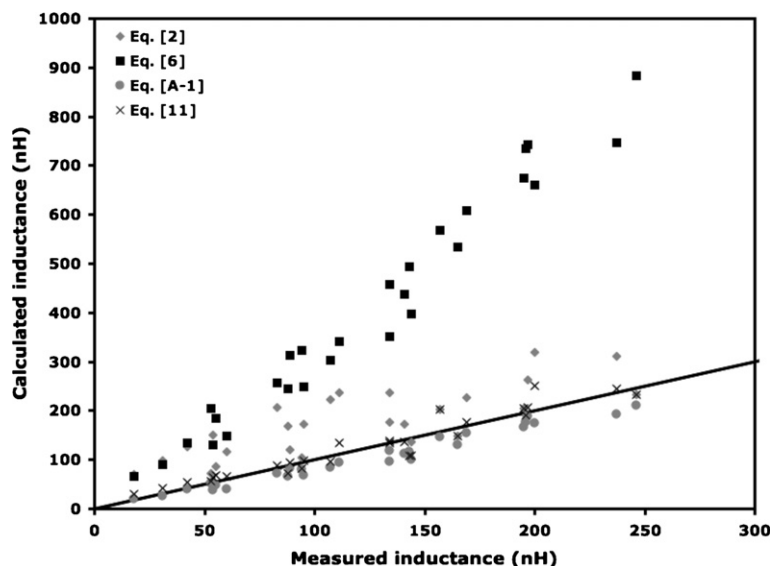
Fig. 4. Measured vs. calculated inductance for a series of 29 flat-coils (Table 1). Measurements were carried out using the circuit shown in Fig. 2 as calibrated in Fig. 3; calculations were carried out using the indicated inductance estimation formulae. The solid line indicates the exact agreement between calculation and measurement.

26% error or better (magnitudes of error for these 5 coils were 5–25 nH).

2.5. Practical testing of flat-coils

For a Chemagnetics Apex DRNS Wideline static probe (Varian Associates, Fort Collins, CO) operating at 300 MHz for the ^1H channel, the two solenoidal coils provided by the manufacturer were a 5 mm coil (5-2, Table 2; estimated inductance (L_{est}) $\sim$ 113 nH) and a 10 mm coil (10-1, Table 2; $L_{est} \sim$ 170 nH). Coils F9-2 ($L_{est} \sim$ 208 nH), F4-2 ($L_{est} \sim$ 135 nH), and F4-4 ($L_{est} \sim$ 99 nH) were designed for, and work with, this probe. (Note that values of L_{est} are given for the required lead-to-lead length of 11.75 mm for the probe, as opposed to the lengths reported in Tables 1 and 2.) In general, each of these three flat-coils tunes and matches very satisfactorily in the probe circuit with the same capacitor ranges for varying heteronuclei as the corresponding solenoidal coil. As might be anticipated, coil F-8 has a slightly different tuning range than the 10 mm solenoid provided by the manufacturer, but has still performed well with all solid-supported oriented lipid bilayer samples we have examined to date.

In the case of a Varian/Chemagnetics T3 narrowbore HX PISEMA probe (Varian Associates) operating at a ^1H-frequency of 600 MHz, the two coils provided by the manufacturer were a 5 mm solenoid (5-4, Table 2; $L_{est} \sim$ 62 nH) and a 4-turn flat-coil (F5-3; $L_{est} \sim$ 57 nH). In order to increase the allowable sample width with a flat-coil, we estimated dimensions that would provide a similar inductance (F11; $L_{est} \sim$ 68 nH); this coil indeed provides very similar tuning and matching performance in comparison to coils F5-3 and 5-4. Note that Eq. (6)

would be completely ineffective in this estimation, since the inductance ranges it estimates are $\sim 3\times$ the real values. Therefore, we have found Eq. (11) to be extremely useful for selection of the number of turns and fine-tuning of coil dimensions without the need for building and testing of numerous coils.

2.6. Examining solenoids with similar inductance but different inner diameter

Use of NMR coils with different diameters is common for solution-state as well as solid-state NMR. In cases where sample is limited, going to smaller coil diameter assists by increasing concentration through the decreased volume required to fill the coil (see e.g. [15] for extensive discussion). Using a Varian T3 PISEMA static solid-state NMR probe operating on an INOVA 600 MHz spectrometer (Varian Associates, Palo Alto, CA), we have compared performance of four coils shown in Fig. 6: 5-4 (6-turn, 5.0 mm id, $L_{obs} \sim$ 55 nH, $L_{estimate}$ 62 nH), 3-1 (9-turn, 3.2 mm id, $L_{obs} \sim$ 56 nH, $L_{estimate}$ 56 nH), 2-1 (14-turn, 1.9 mm id, $L_{obs} \sim$ 66 nH, $L_{estimate}$ 49 nH), and 1-2 (23-turn, 1.1 mm *id*, $L_{obs} \sim$ 56 nH, $L_{estimate}$ 49 nH). Each coil has similar measured and estimated inductance, but different diameter and number of turns, allowing direct comparison of performance in the NMR probe of coils with different diameter. Using neat water as a sample in a tube of the maximum possible diameter, we compared applied RF-field strength (90° pulse width; γB_1) and integrated signal area per millimol of water. Note that peak area for identically acquired and processed spectra provides a direct, linewidth independent measure of sensitivity, since we observed identical noise amplitude for all four coils. Since tube wall thickness becomes increasingly

Table 2
Solenoid dimensions and number of turns alongside measured inductances used to determine suitability of solenoidal inductance estimation formulae

Coil label	N	id (mm)	l (mm)	Inductance (nH)[a]
10-1[b]	5	10.3	14.4	161 ± 3[c]
8-1	4	8.3	5	122 ± 0.2
8-2	4	8.3	10.2	84 ± 1
6.5-1	6	6.5	11.6	127 ± 0.9
6.5-2	5	6.6	12.0	76 ± 0.3
6.5-3	4	6.6	11.2	48 ± 0.4
5-1[d]	6	5.0	1.8	224 ± 0.4[c]
5-2[b]	8	5.3	14.4	129 ± 3
5-3	6	4.9	10.2	72 ± 0.5
5-4	6	5.0	12	55 ± 3
5-5	5	5.0	11.2	45 ± 0.8
5-6	4	4.9	11.9	25 ± 2
3.5-1	10	3.5	12	76 ± 2
3.5-2	8	3.5	12	50 ± 1
3.5-3	6	3.5	11.0	31 ± 3
3.5-4	5	3.5	11.5	19 ± 2
3-1	9	3.2	12	56 ± 0.1
2.5-1	12	2.4	15	50 ± 2
2.5-2	10	2.4	12	36 ± 1
2-1[e]	14	1.9	12.6	66 ± 3
2-2[e]	17	1.9	21.2	44 ± 1
2-3[e]	15	1.9	20.5	33 ± 3
1-1[f]	25	1.0	12	58 ± 0.4
1-2[f]	23	1.1	12	56 ± 0.1

Unless otherwise indicated, all coils were fabricated with 20 AWG copper wire.

[a] Errors are given based upon the paired measurements made at high and low total capacitance for the measurement circuit. Uncertainty in inductance measurement is ∼20–30 nH. Unless otherwise noted, inductance calibrated by linear regression over 0–150 nH range of inductors (Fig. 3).

[b] 19 AWG silver wire.

[c] Inductance calibrated by linear regression over 0–1.0 μH range of inductors (Fig. 3).

[d] 32 AWG copper wire.

[e] 22 AWG copper wire.

[f] 26 AWG copper wire.

crucial with smaller diameter coils, the peak area per molecule normalized by the filling factor of the coil was compared. Fig. 6 shows these measures for each of the four coils tested as labelled with nominal id's of 1, 2, 3 and 5 mm.

Fig. 6 demonstrates a direct–linear relationship between the γB_1 and sensitivity. Note that this is an inverse relationship to coil diameter (for coils of similar inductance), demonstrating an ∼10 fold-increase in sensitivity for a 1 mm coil vs. a 5 mm coil if filling-factor is taken into account. This is on the same order of magnitude as the increases observed with microflow NMR, where smaller sample volumes (∼1.5 μL nominal observe volume) are employed [15]. Note that in this latter case, a customized probe is used due to the requirements of liquid flow through the coil. In work on microcoils, an ∼10–12-fold increase in signal-to-noise has been observed for a decrease in diameter from 1 mm to 100 μm [11,12]. At these dimensions, skin effects become increasingly important, however, and signal-to-noise increases ∼logarithmically with decreased diameter rather than linearly. Here, we use the same static

solid-state NMR probe for all measurements which makes direct comparison of coil capabilities possible and demonstrates the utility of <10 μL volume coils in a standard probe.

2.7. Quick-reference guide to practical coil design for an existing probe

The following process is our recommended design protocol for introducing new coils into an existing probe. In order to make this process rapid for any laboratory, we have produced a spreadsheet for Microsoft Excel allowing side-by-side comparative calculation of inductance estimates for flat- and solenoidal radiofrequency NMR coils of many geometries based on the equations recommended in this paper (freely available at http://structbio.biochem.dal.ca/jrainey/).

(1) Calculate estimated inductances of existing coil(s) (Eqs. (11) and (12)), making note appropriate capacitor combinations for any exchangeable capacitors in the probe.
(2) Optimize number of turns, length, and cross-sectional dimensions of new coil based on sample size (Eq. (11) or (12)). Knowing multiple useable inductance values (i.e. coils that operate with different sets of exchangeable capacitors) may be useful at this point, since a given sample may be more readily wrapped in a coil designed to have one inductance vs. another. However, one should also take into special consideration that the coil does not self-resonate [8,16] at or near the desired operating frequency of the probe as this will affect probe tuning and efficiency.
(3) Fabricate coil and test its performance in the probe using a sweep generator and oscilloscope, the spectrometer tuning circuitry, or other standard method.

3. Conclusions

Although desirable for allowing study of diverse sample types by a given NMR probe, the calculation of inductances for radiofrequency flat-coils is not trivial. We present a comparison of a variety of inductance estimation formulae with measured inductances obtained using a straightforward inductance measurement method relying upon instrumentation available in many NMR laboratories rather than more specialized, and costly, instruments often employed in the literature. Estimation methods are presented which have proven very useful for fabrication of new coils in our laboratory under a variety of cases in two different static solid-state NMR probes operating at ^{1}H frequencies of 300 and 600 MHz. A direct comparison of the performance in an NMR spectrometer of solenoidal coils with very similar measured and estimated inductances but different inner diameters is also presented.
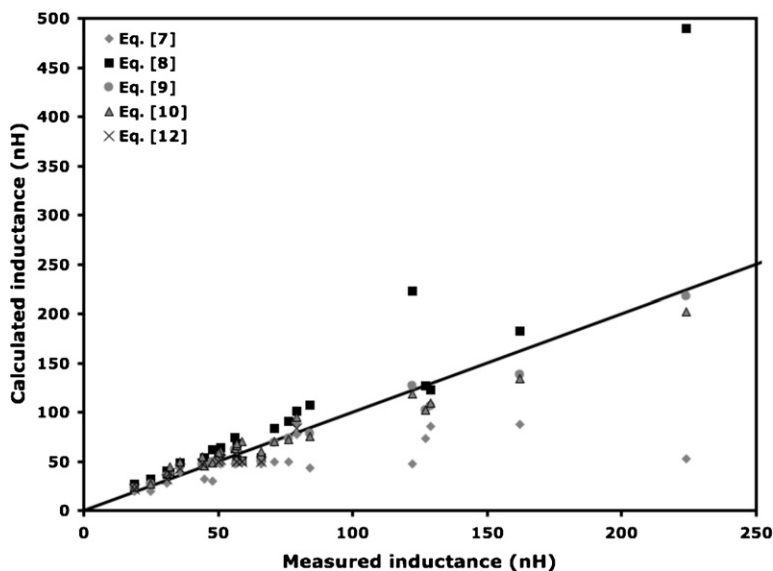
Fig. 5. Measured vs. calculated inductance for a series of 24 solenoidal coils (Table 2). Measurements were carried out using the circuit shown in Fig. 2 as calibrated in Fig. 3; calculations were carried out using the indicated inductance estimation formulae. The solid line indicates the exact agreement between calculation and measurement.
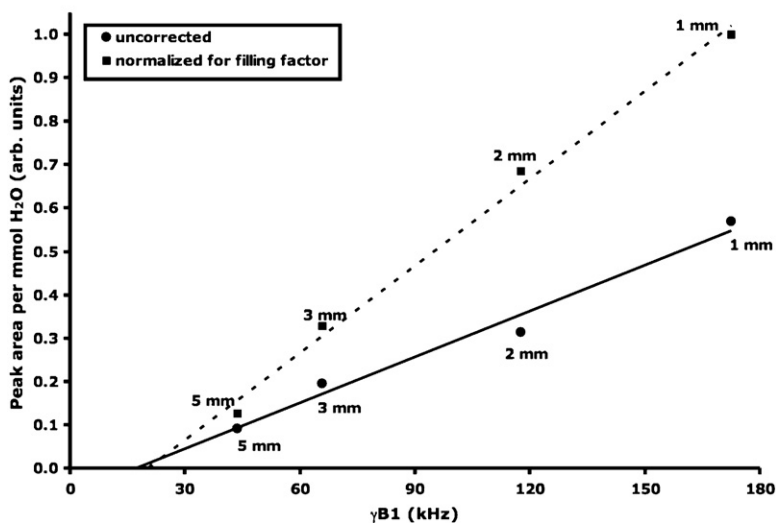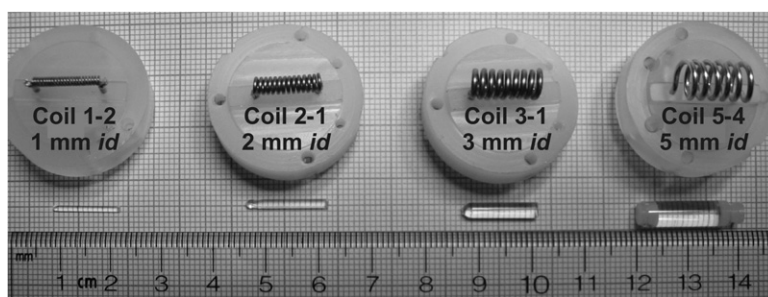

Fig. 6. Coil sensitivity in form of observed peak area for water samples in shown solenoidal coils of given nominal inner diameter. All coils demonstrated identical noise amplitude. Solid line is linear fit to uncorrected area per mmol while dashed line is for area per mmol corrected for coil filling factor.

4. Experimental

4.1. Inductance measurement

The circuit illustrated schematically in Fig. 2 was used, where the coil was placed in series with a pair of 5202 var-

iable capacitors (250 WVDC, Johanson Manufacturing Corporation, Boonton, NJ, USA) (C_A and C_C; ranges 0.8–12.1 pF and 0.8–11.9 pF) and in parallel with a third (C_B; range 0.8–12.2 pF) to create a simple matched tank circuit. A 50 Ω load terminated the circuit at the ground plane to ensure proper loading of the circuit. An SG-677/U

sweep generator (Texscan Corporation, Indianapolis, IN, USA) was used to provide a frequency scan over the range 1 MHz–1.2 GHz and the circuit response (tuning/matching/Q performance) was measured through a ZFDC-10-2 directional coupler (Mini-Circuits, Brooklyn, NY, USA) using a model 475A oscilloscope (Tektronix, Beaverton, OR, USA). An alternative configuration made use of a 1–400 MHz sweep generator (Model 1061, Wavetek, Indianapolis, IN, USA). Upon insertion of a new coil into the circuit, the capacitance of C_B was set to both minimum and maximum values. Capacitors C_A and C_C could be varied at each value of C_B to achieve a well resolved and matched maximum in the frequency scan, which provides the resonant frequency of the circuit. In practice, we found that keeping C_A and C_C at their maximum capacitance provided a good match. The range of each capacitor and its rate of variation over that range was calibrated individually using a model 820 BK capacitance meter (B&K Precision Corporation, Yorba Linda, CA, USA) prior to assembly of the circuit. Approximate, total effective capacitance (C_{eff}) of the circuit is given by

$$C_{eff} \approx \frac{C_A C_B + C_B C_C + C_A C_C}{C_A + C_C} \tag{13}$$

as developed in Appendix C. Coil inductance can then be determined approximately given an observed resonance frequency using Eq. (1). To compensate for systematic errors between measured and actual inductance, the circuit was calibrated using a range of 27 inductors of differing specifications with overlapping inductance ranges (6 IM-2 series molded inductors in the range 150 nH–1 μH 10% tolerance, Vishay Intertechnology, Malvern, PA, USA; 8 CM252016 series chip inductors in the range 10–150 nH 10% tolerance and a 1 μH inductor 10% tolerance, 11 CI201210 series chip inductors in the range 12–220 nH 5% tolerance, and one CM160808 chip inductor at 47 nH 5% tolerance, Bourns, Riverside, CA, USA). All inductors were chosen such that their self-resonant frequencies were well above the resonant frequencies being measured.

We found different performance of the circuit at each extreme of capacitor C_B. In each case, the measured inductance arising from Eqs. (1) and (13) was greater than the real inductance. As shown in Fig. 3, each circuit resonance measurement made at the high-frequency end (low capacitance value of C_B) vs. the low-frequency end provided a significantly greater difference between measured and real inductance. Therefore, we calibrated the inductance measurements for each frequency extreme of the resonance circuit separately. Specifically, linear regression of measured vs. actual inductance values was used to provide an expression for corrected value of inductance. As this will be dependent upon the circuit in question, this is not discussed in detail. It is the average of these two corrected values that is reported as the "measured inductance" for all coils examined. For all coils measured with inductance below ~150 nH, linear regression results from the calibration over the range of 0–150 nH were employed; all higher

inductance coils used linear regression results from the entire data set.

Appendix A. Niwa formula for flat-coil inductance

Niwa's formula for a solenoid of N equally spaced turns wound over a length of l on a rectangular former of height h and width w is given by Grover [4] as:

$$
\begin{aligned}
L = 0.008 N^2 \frac{wh}{l} & \left[\frac{1}{2} \frac{l}{h} \sinh^{-1} \frac{w}{l} + \frac{1}{2} \frac{l}{w} \sinh^{-1} \frac{h}{l} - \frac{1}{2} \right. \\
& \times \left(1 - \frac{h^2}{l^2} \right) \frac{l}{h} \sinh^{-1} \frac{w}{l\sqrt{1+h^2/l^2}} - \frac{1}{2} \left(1 - \frac{w^2}{l^2} \right) \sinh^{-1} \\
& \times \frac{h}{l\sqrt{1+w^2/l^2}} - \frac{1}{2} \frac{h}{l} \sinh^{-1} \frac{w}{h} - \frac{1}{2} \frac{w}{l} \sinh^{-1} \frac{h}{w} \\
& + \left(\frac{\pi}{2} - \tan^{-1} \frac{wh}{l^2\sqrt{1+g^2/l^2}} \right) \\
& + \frac{1}{3} \frac{l^2}{wh} \sqrt{1+\frac{g^2}{l^2}} \left(1 - \frac{1}{2} \frac{g^2}{l^2} \right) + \frac{1}{3} \frac{l^2}{wh} - \frac{1}{3} \frac{l^2}{wh} \sqrt{1+\frac{w^2}{l^2}} \\
& \times \left(1 - \frac{1}{2} \frac{w^2}{l^2} \right) - \frac{1}{3} \frac{l^2}{wh} \sqrt{1+\frac{h^2}{l^2}} \left(1 - \frac{1}{2} \frac{h^2}{l^2} \right) \\
& \left. + \frac{1}{6} \frac{l}{wh} \left(\frac{g^3 - w^3 - h^3}{l^2} \right) \right]
\end{aligned} \tag{A.1}
$$

where $g^2 = h^2 + w^2$. Note that based on similarity of terms, it is possible that the fourth term should have a l/w multiplier, however we were unable to obtain the original Niwa paper from 1918 [17] to verify this; comparing calculated inductances for the two forms of the formula, addition of this l/w multiplier reduces inductance estimates by 0.1–1.1 nH.

Appendix B. Derivation of inductance estimates

As mentioned in the main text, we use a fairly fundamental level of electricity and magnetism theory [8]. To begin with, we consider the magnetic field at an arbitrary point in space, P, caused by a conductor. This is defined by the law of Biot and Savart. For an infinitesimally short segment of conductor of length dl, a vector can be defined

in the direction of the current, **dl**. The field at point P induced by a given conductor segment is dependent on the distance from segment dl to P, r, and the direction of the vector between the conductor and P, $\hat{\mathbf{r}}$. The contributions of each conductor segment to the total magnetic field at P, **B$_P$**, are:

$$d\mathbf{B_P} = \frac{\mu_0}{4\pi} \frac{I d\mathbf{l} \times \hat{\mathbf{r}}}{r^2} \tag{A.2}$$

with magnitude given by:

$$|d\mathbf{B_P}| = \frac{\mu_0}{4\pi} \frac{I dl \sin\phi}{r^2} \tag{A.3}$$

where μ_0 is the permeability of free space, I is the current in the conductor, and ϕ is the angle between **dl** and $\hat{\mathbf{r}}$.

For clarity, the terminology used to refer to features of a flat-coil in the following derivation is illustrated in Fig. 1. To allow the integration to be independent of the number of turns in the coil, we simplify the geometry of the coil such that we have a series of parallel rectangles separated from each other by distance s. Conductor width is also taken to be nonexistent and skin effects [9,17] are not taken into account. The magnitude of the magnetic field caused by one turn (i.e. one rectangle of conductor) of the coil at some arbitrary distance z along the centre-line of the coil may be determined by substitution of the following equations into Eq. (A.3). First, for the top and bottom conductors:

$$\sin\phi = \sqrt{\frac{z^2 + (h/2)^2}{r^2}} \tag{A.4}$$

and

$$r^2 = \left(\sqrt{(x - 1/2w)^2 + z^2}\right)^2 + (h/2)^2 \tag{A.5}$$

where x varies between $-1/2w$ and $1/2w$. Integrating Eq. (A.3) with Eqs. (A.4) and (A.5) substituted in over $x = -1/2w$ to $1/2w$ gives:

$$B_{\text{top}} = B_{\text{bot}} = \frac{\mu_0 I}{\pi} \left(\frac{w}{\sqrt{(4z^2 + h^2)(4z^2 + w^2 + h^2)}} \right) \tag{A.6}$$

Note that the direction of the current is reversed in top versus bottom while the integration direction is also reversed in top versus bottom giving an identical solution for each. Second, for the left and right conductors:

$$\sin\phi = \sqrt{\frac{z^2 + (w/2)^2}{r^2}} \tag{A.7}$$

and

$$r^2 = \left(\sqrt{(y - 1/2h)^2 + z^2}\right)^2 + (w/2)^2 \tag{A.8}$$

where y varies between $-1/2h$ and $1/2h$. Integrating Eq. (A.3) with Eqs. (A.7) and (A.8) substituted in over $y = -1/2h$ to $1/2h$ gives:

$$B_{\text{left}} = B_{\text{right}} = \frac{\mu_0 I}{\pi} \left(\frac{h}{\sqrt{(4z^2 + w^2)(4z^2 + w^2 + h^2)}} \right) \tag{A.9}$$

where reversal of the sign of I applies for the left versus right side, giving identical values for each side. The total value of the magnetic field arising from the contributions of a given rectangular turn of the coil separated from point P by distance z along the coil centre-line is then given by the summation of Eqs. (A.6) and (A.9) multiplied by 2 to give contributions for each of the four sides of the rectangle:

$$B_{\text{turn}}(z) = \frac{2\mu_0 I}{\pi} \left(\frac{w}{\sqrt{(4z^2 + h^2)(4z^2 + w^2 + h^2)}} \right.$$
$$\left. + \frac{h}{\sqrt{(4z^2 + w^2)(4z^2 + w^2 + h^2)}} \right) \tag{A.10}$$

If the turns are separated by a uniform distance s (Fig. 1) the total magnetic field at the centre of the coil is given by the following sum:

$$B = \frac{2\mu_0 I}{\pi} \sum_{n=lb}^{ub} \left(\frac{w}{\sqrt{(4ns^2 + h^2)(4ns^2 + w^2 + h^2)}} \right.$$
$$\left. + \frac{h}{\sqrt{(4ns^2 + w^2)(4ns^2 + w^2 + h^2)}} \right) \tag{A.11}$$

where lb and ub are given by

$$lb = -((N-1)/2)$$
$$ub = ((N-1)/2) \tag{3}$$

for an odd number of turns N, and

$$lb = -((N-2)/2)$$
$$ub = (N/2) \tag{4}$$

for an even N. These different limits keep the calculation in the centre of a turn closest to the middle of the coil.

We now make use of the fact that the total energy supplied by a current increase from 0 to I to an inductor with inductance L is given by:

$$E = 1/2LI^2 \tag{A.12}$$

while the energy stored per unit volume of an inductor is:

$$e = \frac{B^2}{2\mu_0} \tag{A.13}$$

We now get an approximation of the total energy of the coil at current I by multiplying Eq. (A.13) by the volume

of the rectangular coil, which can be equated to Eq. (A.12) giving:

$$1/2 L I^2 \approx \frac{B^2 (hw[N-1]s)}{2\mu_0} \qquad (A.14)$$

Solving for L and substituting Eq. (A.11) for B provides an estimation of coil inductance purely in terms of the number of turns of the coil and its dimensions:

$$
\begin{aligned}
L \cong {} & \frac{4\mu_0}{\pi^2} (hw[N-1]s) \\
& \times \left[\sum_{n=lb}^{ub} \left(\frac{w}{\sqrt{(4(ns)^2 + h^2)(4(ns)^2 + w^2 + h^2)}} \right. \right. \\
& \left. \left. + \frac{h}{\sqrt{(4(ns)^2 + w^2)(4(ns)^2 + w^2 + h^2)}} \right) \right]^2
\end{aligned} \qquad (2)
$$

A similar analysis may readily be carried out for a solenoidal coil with circular turns. The total magnetic field at the centre of the coil is given by

$$B = \frac{\mu_0 I r^2}{2} \sum_{n=lb}^{ub} \left(\frac{1}{((ns)^2 + r^2)^{3/2}} \right) \qquad (A.15)$$

where r is the radius of the circular coil, and n, and s retain the same meaning as for the rectangular coil and the lb and ub are given by Eqs. (3) and (4) for odd and even N, respectively. Substitution into Eq. (A.15) provides the following estimate of inductance

$$L \cong \frac{\mu_0 \pi r^6 [N-1]s}{4} \left[\sum_{n=lb}^{ub} \left(\frac{1}{((ns)^2 + r^2)^{3/2}} \right) \right]^2 \qquad (7)$$

Appendix C. Circuit capacitance calculation

If we make the simplifying assumption that the inductance measurement tank circuit (Fig. 2) has no resistance, the total impedance (Z_T) at a given frequency ω of the circuit contains only imaginary components:

$$
\begin{aligned}
Z_T &= Z_{C_A} + \left(\frac{1}{Z_{C_B}} + \frac{1}{Z_L} \right)^{-1} + Z_{C_C} \\
&= \frac{1}{j\omega C_A} + \left(j\omega C_B + \frac{1}{j\omega L} \right)^{-1} + \frac{1}{j\omega C_C}
\end{aligned} \qquad (A.16)
$$

When the circuit is at resonance, Eq. (1) applies (note that ω is in units of rad/s, as opposed to in Hz) and the total impedance will be zero. Rearrangement of Eq. (A.16) under the resonance condition provides the

following expression for the total effective capacitance of the circuit:

$$C_{\mathrm{eff}} \approx \frac{C_A C_B + C_B C_C + C_A C_C}{C_A + C_C} \qquad (13)$$

Appendix D. Supplementary data

Supplementary data associated with this article can be found, in the online version, at doi:10.1016/j.jmr. 2007.03.016.

References

[1] B. Bechinger, S.J. Opella, Flat-coil probe for NMR spectroscopy of oriented membrane samples, J. Magn. Reson. 95 (1991) 585–588.
[2] R. Freeman, A Handbook of Nuclear Magnetic Resonance, Addison Wesley Longman, Harrow, Essex, England, 1997.
[3] M.T. Thompson, Inductance calculation techniques—part I: classical methods, Power Control and Intelligent Motion 25 (1999) 40–45.
[4] F. Grover, Inductance Calculations, D. Van Nostrand Company, New York, 1946.
[5] J.C. Ginefri, E. Durand, L. Darrasse, Quick measurement of nuclear magnetic resonance coil sensitivity with a single-loop probe, Rev. Sci. Instrum. 70 (1999) 4730–4731.
[6] A. Leroy-Willig, L. Darasse, J. Taquin, M. Sauzade, The Slotted cylinder—an efficient probe for NMR imaging, Magn. Reson. Med. 2 (1984) 20–28.
[7] M.H. Levitt, Spin Dynamics—Basics of Nuclear Magnetic Resonance, Wiley, New York, 2001.
[8] H.D. Young, University Physics, eighth ed., Addison-Wesley, Reading, MA, 1992.
[9] H.A. Wheeler, Formulas for the skin effect, Proc. I.R.E. 30 (1942) 412–424.
[10] F.D. Doty, Probe design and construction, in: D.M. Grant, R.K. Harris (Eds.), Encyclopedia of NMR, John Wiley, New York, 1996, pp. 3753–3762.
[11] D.A. Seeber, R.L. Cooper, L. Ciobanu, C.H. Pennington, Design and testing of high sensitivity microreceiver coil apparatus for nuclear magnetic resonance and imaging, Rev. Sci. Instrum. 72 (2001) 2171–2179.
[12] T.L. Peck, R.L. Magin, P.C. Lauterbur, Design and analysis of microcoils for NMR microscopy, J. Magn. Reson. B 108 (1995) 114–124.
[13] Y. Li, A.G. Webb, S. Saha, W.W. Brey, C. Zachariah, A.S. Edison, Comparison of the performance of round and rectangular wire in small solenoids for high-field NMR, Magn. Reson. Chem. 44 (2006) 255–262.
[14] P.L. Gor'kov, E.Y. Chekmenev, R. Fu, J. Hu, T.A. Cross, M. Cotten, W.W. Brey, A large volume flat coil probe for oriented membrane proteins, J. Magn. Reson. 181 (2006) 9–20.
[15] D.L. Olson, J.A. Norcross, M. O'Neil-Johnson, P.F. Molitor, D.J. Detlefsen, A.G. Wilson, T.L. Peck, Microflow NMR: concepts and capabilities, Anal. Chem. 76 (2004) 2966–2974.
[16] L.D. Wolfgang, C.L. Hutchinson (Eds.), The ARRL Handbook for Radio Amateurs, 16th ed., The American Radio Relay Leauge, Newington, CT, 1991.
[17] Y. Niwa, Unknown, Researches of the Electrotechnical Laboratory 73 (1918).